Geo-Mar Lett (2015) 35:237–246
DOI 10.1007/s00367-015-0403-9

ORIGINAL

Mud volcanoes and evaporite seismites in a tidal flat of northern Kuwait—implications for fluid flow in sabkhas of the Persian (Arabian) Gulf

Michael J. Duane[1] · **Linda Reinink-Smith**[1] · **Christopher Eastoe**[2] · **Ali T. Al-Mishwat**[1]

Received: 1 February 2015 / Accepted: 16 March 2015 / Published online: 25 March 2015

Abstract This paper reports the first interpretative field map and stable isotope geochemistry of an exhumed Miocene inlier with conical mud volcanoes in a Persian (Arabian) Gulf salt flat (sabkha). In Kuwait, the siliciclastic low-heat flow margin of the northern gulf sector produced sedimentary conditions with numerous multilayered, unstable density gradients that were highly susceptible to recording liquefaction effects. The geotechnical characteristics of the sabkhas and the effects of local seismic activity resulted in ideal conditions in marginal sediments of Kuwait Bay, well suited for the development of deformation features. Three-dimensional, pseudo-biohermal exposures exhibit ellipsoidal pillows with craters separated by fluidized channels of chaotic orientation. The size and morphology of these structures together with cogenetic mud volcanoes are strongly influenced by sedimentary factors such as density gradients and tectonic events such as localized seismic activity, which caused mixing of fluids. Diapirs emerged concurrently with syn-sedimentary deformation, and the mud injection responded to episodic seismic activity. Interpretation based on previously published reflux models such as evaporative pumping and seawater flooding of coastal sabkhas is not applicable in this case. Rather, a model of focused ascent of brine initiated by episodic seismicity is proposed. Swarms of mud volcanoes represent new abiotic sedimentary features in sabkhas, but the per-ascensum nature of the fluid offers some comparisons to siliceous hot-water vents in south-eastern Brazil.

Michael J. Duane holds a PhD at Kuwait University.
Linda Reinink-Smith holds a PhD at Kuwait University.
Christopher Eastoe holds a PhD at University of Arizona.
Ali T. Al-Mishwat holds a PhD at Kuwait University.

✉ Michael J. Duane
phytokarst@gmail.com

[1] Department of Earth & Environmental Sciences, Kuwait University, P.O. Box 5969, Safat 13060, Kuwait

[2] Department of Geosciences, University of Arizona, Tucson, AZ, USA

Introduction

Mud volcanoes occur in a wide variety of geological environments that permit escape of focused fluid from sedimentary basins. The geological field descriptions for feeder complexes are sparse (Davies and Stewart 2005; Roberts et al. 2010), as are the injection effects on local stratigraphy (Castilla and Audemard 2007). The geological definition of a mud volcano (Stewart and Davies 2006) requires the presence of a set of structures associated with an extrusive edifice and subaqueous plumbing system, which connects to a stratigraphic subsurface source. The geometries of these stratigraphic connectors have been described as diatremes (Robertson and Kopf 1998), vertical pipes (Graue 2000), mud pipes, dyke-sill complexes (Morley 2002; Stewart and Davies 2006) and conical mounds (Yamamoto et al. 2005).

Mud volcanoes develop mostly in convergent orogens but also in deltaic settings (e.g. the Nile delta; Loncke et al. 2004; Feseker et al. 2010; Dupré et al. 2014). In the present case, the first observation of sulphate-silica mud diapirs from an arid sabkha setting in the Persian Gulf is described. Detailed mapping of the shallow subsurface zones of sabkha-intrusive mud volcanoes is expected to elucidate the processes that govern fluid transport through the shallow sub-surface, thereby leading to improved modelling of seismic events in evaporitic stratigraphy records. In the Persian Gulf region, the Arabian plate is moving northeast against the Eurasian plate (Authemayou et al. 2006). The region is not recognized as a

mud volcano environment, but compressional forces lead to pervasive gas venting on the seafloor (Uchupi et al. 1996). Onshore salt tectonics are known to occur in the Iranian sector of the Persian Gulf bordering the Sea of Oman, and favourable conditions for the development of sub-aerial mud volcanoes can therefore be expected (Negaresh and Khosravi 2008). However, there are few, if any, mud volcanoes reported from low-temperature salt-flat environments preserved together with siliceous sediments (cf. Grasby et al. 2009).

The main aim of the present study, therefore, was to describe the pseudo-stromatolithic features observed in the siliciclastic tidal flats of Kuwait Bay in northern Kuwait (Fig. 1) together with their petrography and isotope geochemistry, and to evaluate their combined influence on the geomorphology of this salt-flat environment. A secondary aim was to generate criteria for assessing the genesis of laminar structures and bioherms in sabkhas in general. Indeed, laminar bedding structures in tidal flats are commonly classified as algal and/or microbial in origin (Kendall and Skipwith 1968; Gerdes and Krumbein 1987; Gaillard et al. 1992) but, in fact, may be partly induced by liquefaction in areas of co-eval seismic activity.

Geological setting

A compressional tectonic regime in eastern Kuwait has been maintained since the Tertiary resulting in the formation of the Burgan Arch, a regional anticline bordering the study area. This anticlinal crest confines some of the largest hydrocarbon accumulations in the world (>60 bbs oil) and, like many other oilfields, has a component of thermogenic gas seepage. Mud volcanoes associated with evaporites are a new discovery, having not previously been reported from Arabian tidal-flat environments in spatial association with the eastern flank of the Burgan anticline. The majority of the onshore seismites and mud volcano outcrops are developed in sediments of the Miocene Ghar to lower Fars formations (Figs. 1 and 2), which are equivalents to the Ahwas sandstone member of the Asmari Formation of Iran/Iraq where marginal deposits were developed in sediments of Miocene age (Mukhopadhyay et al. 1996).

The tidal-flat deposits along the coast of Kuwait Bay form an extensive arc of sabkhas deposited on a shallow ramp structure (Fig. 1). The sediments have been exposed to continuous flooding cycles since at least the Late Miocene. They consist of fine-grained evaporites and incorporate a considerable amount of aeolianite (carbonate-cemented wind-blown sands) and stromatolithic structures (Al-Shuaibi et al. 2012; Fig. 1). The present-day onshore mud volcanoes in Kuwait extrude through partially eroded sedimentary highs and pierce through Holocene strata in a NW–SE trend, oblique to the regional sedimentary arc.

Materials and methods

Three well-defined units were identified within the evaporites in the course of a field mapping exercise (zones 1, 2 and 3;

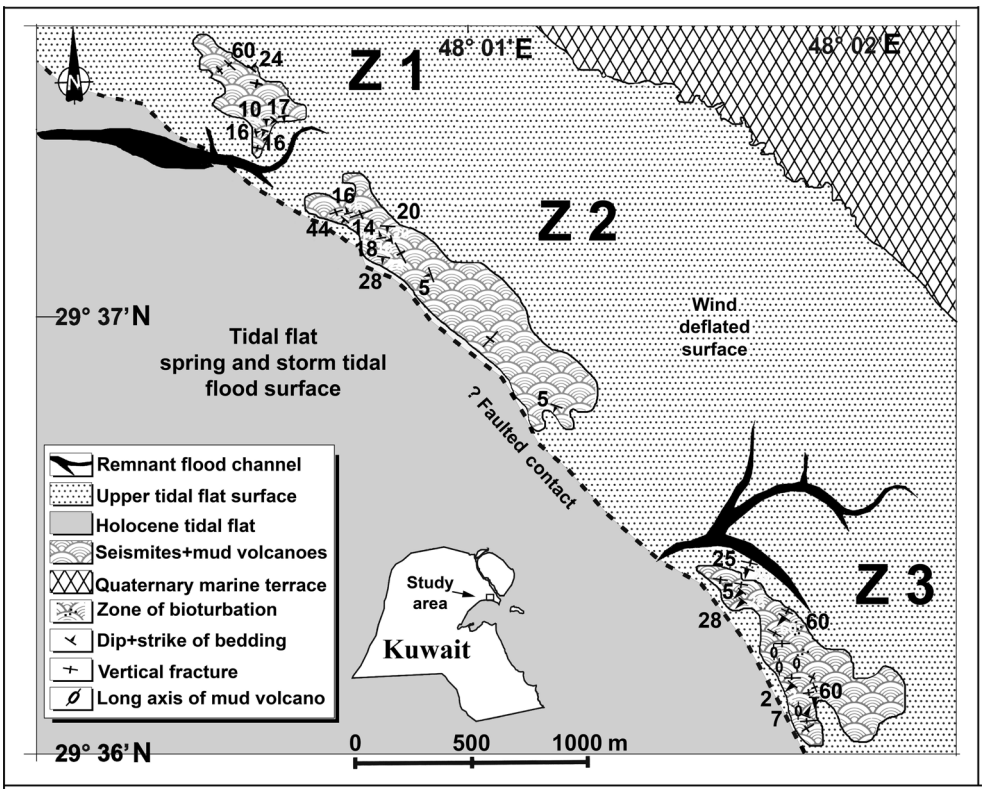

Fig. 1 Geological map of mud volcanoes, small craters and seismites in northern Kuwait. Note that the swarm of newly identified features is confined to three zones: *zone 1* NW sector of exposed Quaternary beach, *zone 2* centre of field, *zone 3* SW sector

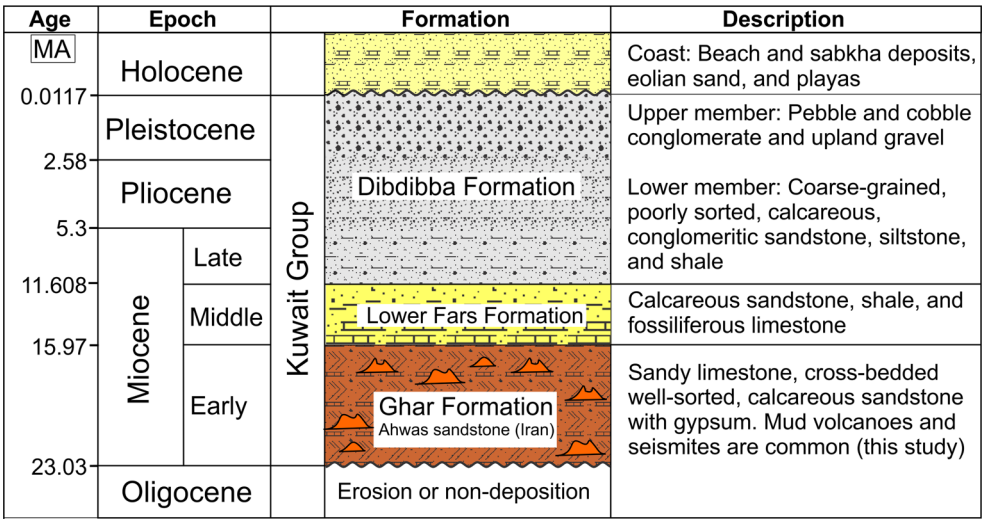

Fig. 2 Stratigraphic column of the main units within the study area. Ghar Formation sediments are the main hosts of the mud volcanoes but the seismites are increasingly observed in younger formations

Fig. 1). Only complete exposures were mapped, and extensions beneath Dibdibba gravel deposits to the north are expected to become exposed in the future as wind deflation of the sabkha continues. Grid mapping was carried out using a handheld global positioning system, and structural readings were measured with a compass clinometer and metre rule. Mud volcano samples were collected and processed for thin sections, and XRD mineral identification was carried out using a Bruker D8 X-ray instrument.

Carbonate isotopes were measured on powdered bulk calcite samples, handpicked from veins and disseminated dolomite. $\delta^{18}O$ and $\delta^{13}C$ of the carbonate material were determined by means of an automated preparation device (KIEL-III) coupled to a Finnigan Mat 252 gas ratio mass spectrometer. Powdered samples were reacted with phosphoric acid under vacuum at 70 °C. The measured isotope ratios are calibrated based on repeated measurements of NBS-19 and NBS-18, with precision of ±0.1‰ for $\delta^{18}0$ and ±0.08‰ for $\delta^{13}C$ (1σ). To test for the effect of any fine-grained calcite present in the bulk rock samples, three samples were reacted quickly with HCl prior to analysis in the Kiel device. The results obtained were identical with those for the corresponding splits that had not been reacted with HCl. The data presented here are therefore considered to represent dolomite, except in cases where there was evidence of calcite veining.

Sulphate from gypsum was extracted from bulk rock samples by leaching with dilute HCl and precipitated as $BaSO_4$. $\delta^{34}S$ was measured on SO_2 gas in a Thermo Quest Finnigan Delta PlusXL continuous flow gas ratio mass spectrometer. Samples were combusted at 1,030 °C with O_2 and V_2O_5 using an elemental analyser (Costech) coupled to the mass spectrometer. Standardization was based on international standards OGS-1 and NBS 123, and several other sulphide and sulphate materials that have been compared between laboratories. Calibration is linear in the range from –10 to +30‰. Precision is estimated to be ±0.15 or better (1σ), based on repeated runs on internal standards. $\delta^{18}O$ of sulphate was measured on CO gas in a Thermo Electron Delta V continuous flow gas ratio mass spectrometer. Samples were combusted with excess C at 1, 350 °C using a thermal combustion elemental analyser (Thermo Quest Finnigan) coupled to the mass spectrometer. Standardization was based on the international OGS-1 standard. Precision was estimated to be ±0.4‰ or better (1σ), based on repeated internal standards. Stable isotope ratios are reported relative to the VPDB (Vienna PDB) standard for carbonates, and VSMOW and VCDT for sulphates.

Results

Geological aspects of mounds

The plan view of the mud volcano system is broadly linear and can be subdivided into three distinct units (zones 1, 2 and 3; Fig. 1), separated by remnant tidal channels. A complete lack of vegetation, due to wind deflation, has fully exposed the structures. The boundary of the area is defined by the edge of the tidal flat that appears to coincide with a sharp and steep (faulted) contact zone. Fracturing is evident throughout the complex, the most common features being regular, grid-like fractures several metres in length and intersect sinuous fractures following several divergent trends (Fig. 3). Conjugate fractures occur closer to the centre of the swarm of mud volcanoes, such fractures being penetrated by small mud volcanoes 4–6 cm in diameter. Dip and strike of the bedded evaporites are consistent except for local areas of steep dip (zone 3) and highly variable strikes mirroring the chaotic bedding produced by syn-sedimentary deformation. Mud was evidently expelled from the feeder system in the form of watery pulses and precipitated in situ (Fig. 3, panel B1), the mud pulses attesting to significant reactivation within the recent past. Small brecciated sandstone clasts and marine bivalves occur

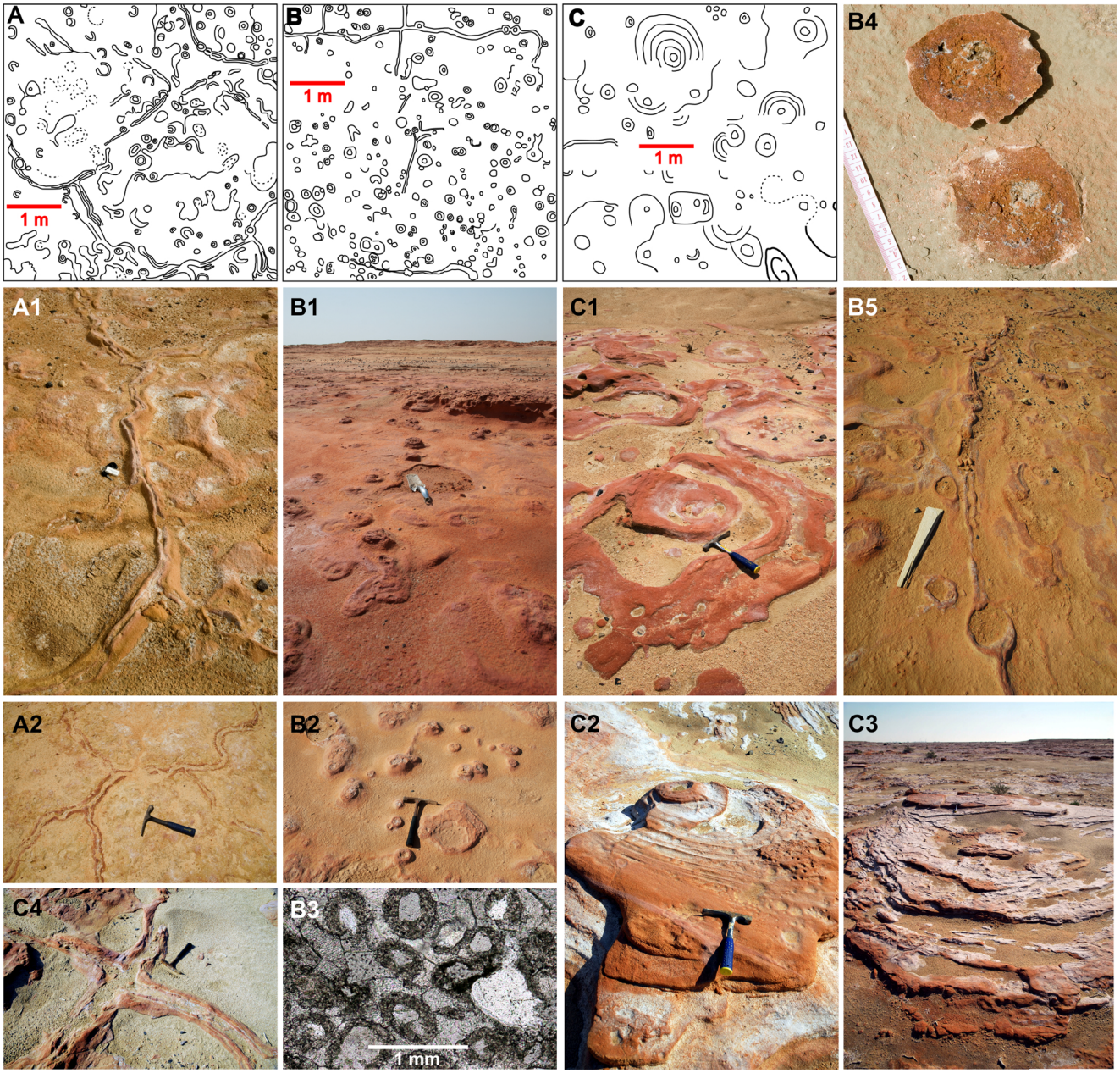

Fig.3 Collage of pertinent geomorphological features, sedimentary structures and micro-features recorded in the tidal flat of Kuwait Bay, including some mapping details. Panels A–C: mapped small-scale features on cemented, flat salt pan; *A* zone 1, *B* zone 2, *C* zone 3 (cf. Fig. 1 and main text)

within the mud matrix. Mapping revealed zones of similar structural elements but with distinct expulsion features. The central zone consists of small craters that range in size from 0.1 cm to 3 m in diameter, often with an ochreous colour contrasting with the surrounding salt-encrusted sabkha. Giant seismites are particularly well developed in zone C. The long axis of the structures (170°) suggests alignment with the ancient channel.

In plan view, isolated pillow structures (individual seismites; Fig. 3, panels C2, C3) occur with elliptical morphology and concentric ring structures, whereas only a few show circular morphology (panel C1). Sizes of pillows are approximately constant within a particular swarm and reach up to 3 m in diameter. The southern sector contains the largest structures (several are >5 m across ellipse axes) with a north–south trend. Mud volcano craters are characteristically perched on the apex of a pillow. Load structures are laterally discontinuous and merge with cemented sabkha material.

The mineralogy of a crater is variable but zoned (Fig. 3, panel B4). Spheroidal dolomite-megaquartz-calcite and occasional lithiophorite [$(Al,Li)MnO_2(OH)_2$] dominate the central core, followed by quartz-gypsum-calcite. The spheroidal dolomites range in size from 5–350 μm and have concentric zones, internal nuclei with or without a radial fabric.

Details of outcrop structures

In the panels of Fig. 3, A, B and C are representative of small-scale features on a cemented, flat salt pan: zone 1 structures = A, zone 2 = B and zone 3 = C. *A*: small prominent craters (diameters <1 cm to 1 m) confined by pseudo-hexagonal sinuous fractures, occasionally penetrated by small craters, are indicative of syn-sedimentary fluid expulsion. *B*: denser pattern of small craters with a tendency to merge and cluster in a chaotic fashion; fractures are discontinuous and appear to be covered by mud. *C*: small craters specifically associated with seismite pillow structures; craters are perched on the apex of the seismites and are associated often with concentric rings, indicating discharge of gas from the pillow.

B4: inverted field specimen showing the interior morphology of a small crater; the presence of vuggy mega-quartz, dolomite and gypsum breccia is characteristic of the apex mud volcano. *B5*: sinuous fracture with small post-development crater penetrating the fracture. *A1, A2, A3*: conjugate syn-sedimentary fractures in zone A; fractures are sealed with megaquartz, calcite, gypsum and flecks of lithiophorite, and were clearly tensional in the early stages of development.

B1: panoramic view of raised terrace showing recently exposed (wind-deflated) platform containing mud volcanoes and fossilized mud flow. *B2*: partly degraded mini cluster of mud volcanoes showing concentric laminae. *B3*: photomicrograph (diameter 25 mm) of dolomitized mud volcano fabric with matrix carbonate and gypsum, enclosing prominent spheroids of dolomite.

C1: giant seismites, weathered with small apex crater in southern zone 3. *C2*: perfectly preserved pillow with deformed aspect and small apex crater common in the southern study area. *C3*: largest observed seismite with an internal diameter of >3 m, displaying a deformed pillow structure.

Trigger mechanism of fluid expulsion

The pillow-like structures illustrated in Fig. 3 were clearly not formed by storm waves because artesian-derived volcanoes are morphologically different, having steeper to near-vertical walls tapering downwards (Mount 1993). Storm-generated waves can be discounted in any case because of the shallow nature and small dimensions of the Persian Gulf during the Miocene. The only probable alternative to seismic-induced liquefaction is overloading of the sediment pile, but this hypothesis can be discounted as well because (1) the units that host the mud volcanoes are shallow near-shore deposits, typically composed of thin laminated sediments; (2) the fact that these structures are laterally continuous in a cross-cutting aspect to the shoreline suggests a local catastrophic geological event; (3) soft-sediment deformation features (Leeder 1987) are found within the evaporites associated with the mud structures; (4) present-day earthquakes are known to occur in the area as a consequence of both oil extraction from the Burgan anticline, and proximity to the active Zagros fold-and-thrust belt; (5) observed sedimentary structures compare well with those generated by liquefaction, not biologically induced sedimentary structures. On the basis of the above considerations, episodic earthquakes are considered to be the most likely trigger mechanism for the fluid expulsion (cf. Fig. 4).

Stable isotope data

Paired $\delta^{34}S$, $\delta^{18}O$ data for gypsum from the study area are plotted in Fig. 5a. Values of $\delta^{34}S$ range from +16 to +23‰, and of $\delta^{18}O$ from –10 to –15‰. Sulphate from zone 1 has lower $\delta^{34}S$ values than that from zones 2 and 3. There is no correlation between $\delta^{18}O$ and $\delta^{34}S$.

Values of $\delta^{13}C$ in dolomite form a triangular array (Fig. 6) and range from –6 to –2‰. $\delta^{18}O$ signatures are –10 to –6‰. Calcite veins plot in the centre of the dolomite field in Fig. 6.

Discussion

Mud volcanoes are usually an expression of mud and fluid eruption at the seafloor (Brown 1990; Kopf 2002; Judd and Hovland 2007) but eruption into a wet sabkha in the Miocene would have produced a unique set of sedimentary structures. The leakage mechanism that drives highly focused, cross-stratal fluid expulsion in sabkha sediments would have involved an enhancement of pressure-generated permeability by hydraulic fracturing (Hubbert and Willis 1957). Several lines of evidence support the pillow-like structures investigated in this study being interpreted as seismites (Seilacher 1969). Relationships between earthquakes and enhanced eruption of mud have been analysed elsewhere (e.g. Deville et al. 2003; Bonini 2009), and are here suggested to be the main trigger mechanism for fluid expulsion.

Hydraulic fracturing can be involved in the early emplacement of sedimentary structures—e.g. remobilization of mud and sand (Van Rensbergen et al. 1999). The studied soft-sediment deformation structures described herein occur at the margin of an elevated Quaternary tidal-flat shoreline. Numerous multilayered unstable density gradients were produced (seawater-mud-evaporites), which is to be expected in evaporative-carbonate systems. Ideal geotechnical conditions were developed during the Miocene to generate large load structures in these previously soft sediments. The origin of the concentric ring structures around the centre of the largest mud volcanoes is considered to be associated with periodic fluctuations in volume flux, where each ring would represent a near-circular mud flow event (Murton and Biggs 2003).

A key feature of the fracture density is its locus that increases from the east to the west, indicating the proximity of the Burgan anticlinal axis. The increasing intensity of the sinuous fracture patterns, on the other hand, points towards the

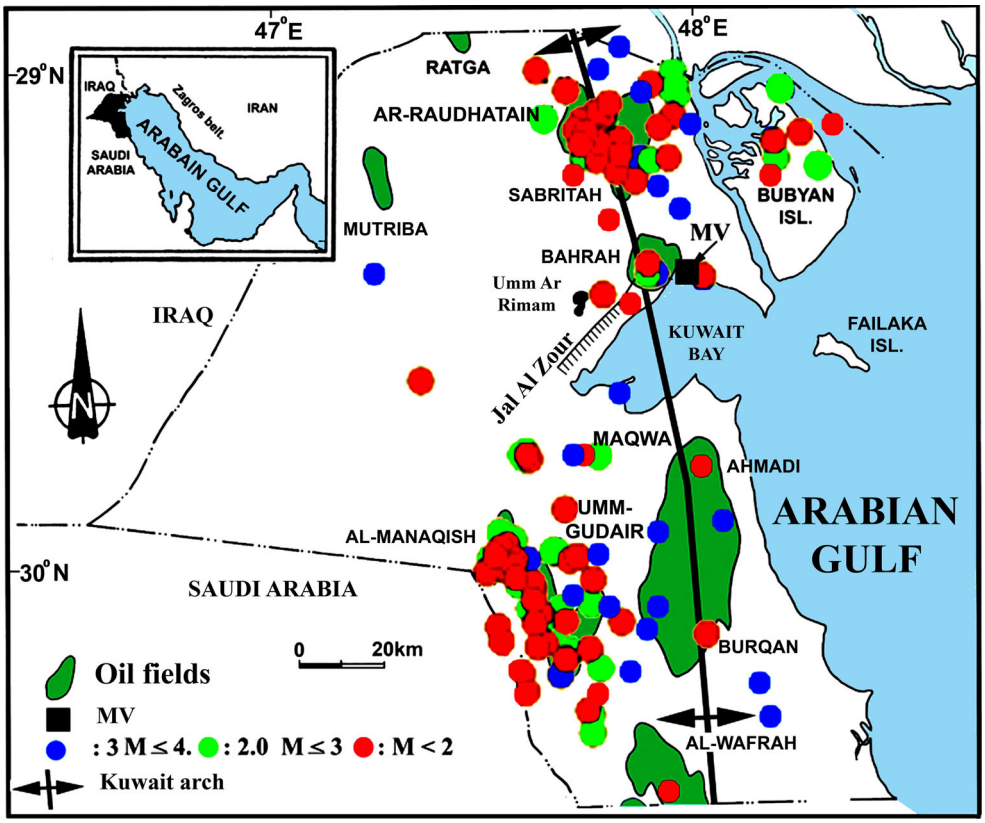

Fig. 4 Compiled seismic and structural data from Kuwait (modified after Sadek 2004). *MV* Mud volcano field, eastern flank of Burgan anticline

original centre of the feeder complex in zone 2, indicating that the mud edifice itself is the principal control on fracture distribution, not the regional folding.

The non-tectonic fractures (those induced by syn-sedimentary deformation of evaporite sediment), on the other hand, may be explained by the mud intrusion process. Overpressured fluids below the edifice would have produced a pressure differential between the fluids in the fractures and the fluids in the sedimentary rocks (Fig. 7). This pressure vector would exceed the minimum principal stress field, causing dilation and fluid flow through the fractures (Morley and Crevello 1998; Jolly and Lonergan 2002; Campbell et al. 2002). Mud drapes in the fracture walls would inhibit exterior fluid leakage and aid in the sustenance of fluid pressure, facilitating fracturing deeper in the pile and the propagation of the fractures up to the surface (Morley 2003).

Fluid sources and mixing trends

Several stable isotope studies of carbonate and sulphate minerals from carbonate formations, active sabkhas along the shoreline of the Persian Gulf and continental getch (gypsum soil enrichment) provide a useful background for the present study (Fig. 6). McKenzie (1981) established that secondary dolomitization of Ca-carbonate sediment in the Abu Dhabi sabkha occurs at temperatures of 34–49 °C. Chafetz et al. (1999) showed the presence of correlatable horizons with low values of $\delta^{18}O$ and $\delta^{13}C$, which they interpreted as evidence of bacterial sulphate reduction (BSR), in Pleistocene dolomites at Al Jubayl (Saudi Arabia). An overlying low-magnesium calcitic facies at Al Jubayl has low values of $\delta^{18}O$ as a result of diagenetic interaction with a lateral influx of meteoric water (Chafetz and Rush 1995). BSR is also considered as an explanation of low values of $\delta^{13}C$ in dolomite of the Eocene Dammam Formation in Qatar, where late influx of meteoric water is the causative agent for overprinting diagenetic calcite (Hanafy et al. 2005). BSR and the presence of sulphate of both marine and continental origin (getch) are inferred from studies of sulphate isotopes in the south and north of Persian Gulf sabkhas (e.g. Olsen 1975; Robinson and Al-Ruwaih 1985; Robinson and Gunatilaka 1991). Furthermore, sulphate is present in groundwater in Kuwait and enters the sabkhas of the south via the Kuwait Group clastics (Robinson and Al-Ruwaih 1985). Those authors identified sulphate with $\delta^{34}S$ values of 15–16‰ in the freshwater entering the sabkha.

Published S isotopic data on the northern Persian Gulf sabkhas indicate a seawater influence ($\delta^{34}S$ of +21‰, $\delta^{18}O$ of +2.4‰) but this applies only in the outer sabkha areas, decreasing towards the landward side. These values are lower than the Abu Dhabi sabkhas where seawater sulphate and BSR are more prevalent, indicating that at least in southern Kuwait the influence of water from continental reflux to the sabkha is greater. Evaluation of the Persian Gulf hydraulic

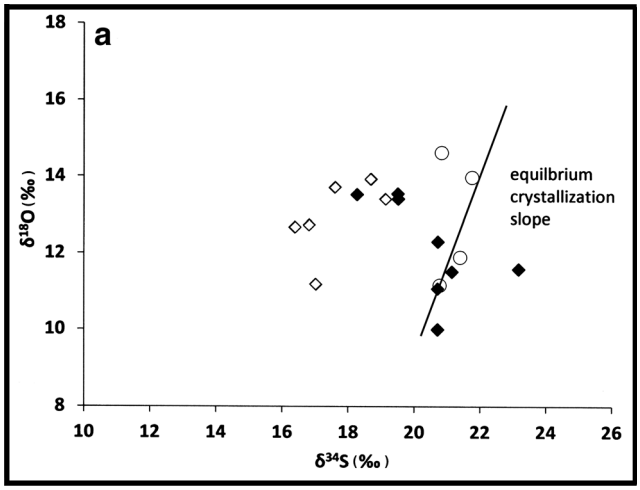

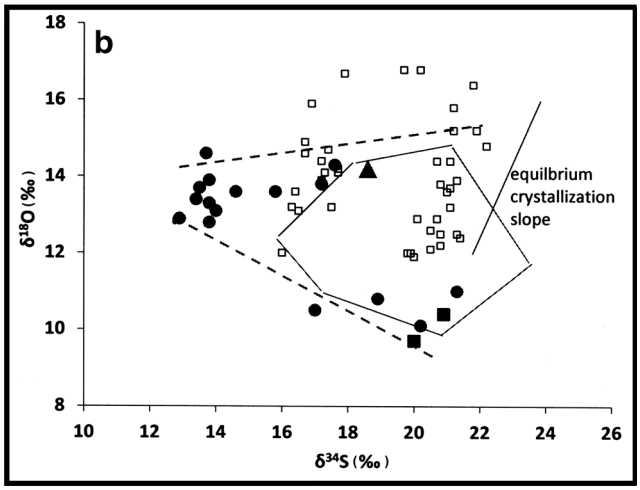

Fig. 5 **a** Mud volcano sulphate isotope data: O vs. S for gypsum from edifice rocks: *open diamond* gypsum A from zone 1, *filled diamond* gypsum B from zone 2, *circle* gypsum C from zone 3. **b** Corresponding data from earlier studies in the Persian Gulf: seawater (Olsen 1975; Robinson and Gunatilaka 1991), continental groundwater from Al-Khiran (southern Kuwait), the Rus anhydrite regional aquiclude together with the regional gypsum getch (Wadi Al Batin surficial deposits), and sabkha minerals from Abu Dhabi (Olsen 1975). *Polygon* Field of data in **a**, *dashed lines* mixing between continental sulphate and evolved seawater (see main text), *continuous line* progressive gypsum recrystallization (Lu et al. 2001), *open square* Abu Dhabi gypsum and anhydrite, *triangle* Rus anhydrite, *circle* Al-Khiran groundwater in southern Kuwait, *closed square* Persian Gulf seawater

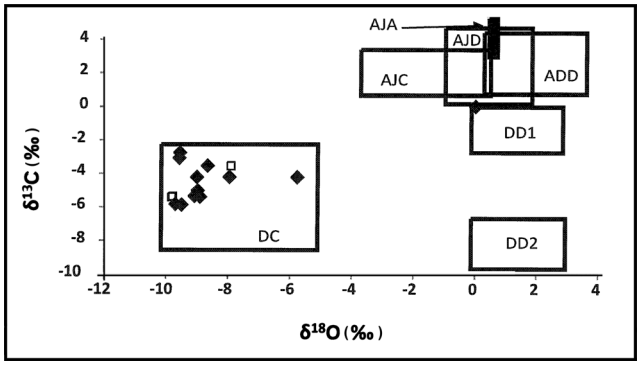

Fig. 6 Plot of oxygen and carbon stable isotopes for dolomite and calcite from the study area, and carbonate stable isotope data from earlier studies of Persian Gulf sabkhas. *AJA, AJC, AJD* Aragonite, calcite and dolomite respectively from Al Jubayl, Saudi Arabia (Chafetz and Rush 1995), *ADD* dolomite, Abu Dhabi (McKenzie 1981), *DD1, DD2, DC* dolomites 1 and 2, and calcite from Dammam Formation, Qatar (Hanafy et al. 2005), *DC* water in equilibrium with Dammam Formation calcite at 60 °C (mineral isotope data from Hanafy et al. 2005). Isotope fractionation data are from Horita (2014) and Ohmoto and Rye (1979)

model for sabkhas (Yechieli and Wood 2002; Wood et al. 2002) suggests that vertical flux of groundwater from the deeper formations could be a major source of solutes (but less so the water), while the seawater influence is confined to a narrow sliver of coastline. The present study supports this model.

Source of sulphate

Figure 5b shows available sulphur isotope data from earlier studies of Persian Gulf sabkhas, along with the $\delta^{34}S$, $\delta^{18}O$ of +14, +13‰ reported by Olsen (1975) and Robinson and Gunatilaka (1991). Another vertex (+20, +10‰) corresponds to present-day Gulf seawater (Olsen 1975; Robinson and Gunatilaka 1991). The third vertex (+22, +15‰), or more positive values, may be related to seawater sulphate. The slope of the data trend between seawater and vertex 3 is too steep to be explained by dissolution and partial recrystallization of gypsum, which would generate a slope near 2 (Lu et al. 2001). The trend is unlikely to represent BSR because there is so little modification of the S isotope signature. A different mechanism for evolving seawater sulphate might involve exchanging O isotopes between evaporite sulphate and mildly oxidizing continental waters in the mixing sub-surface of the edifice mud mounds, but it would be difficult to achieve over a reasonable time scale at temperatures less than 100 °C (Chiba and Sakai 1985). Alternatively, cyclic recrystallization of gypsum in the edifice may be reasonably expected to mix with continental "getch" sulphate, a process ongoing in Kuwait since at least the Miocene. It is possible that such mixing has led to an apparent steepening of a recrystallization trend originating at the seawater vertex, as well as the generation of mixtures in the middle of the triangular array.

During the mid-Miocene, seawater sulphate briefly attained $\delta^{34}S$ values of +22 to +23‰ (Claypool et al. 1980). With the possible exception of sample B6 (zone 2), such sulphate is not evident in the present database. The B6 data could also be explained by invoking BSR. It is not known whether the mud volcanoes were active during that critical part of the Miocene when $\delta^{34}S$ values were high, or at another time when the $\delta^{34}S$ values of marine sulphate were closer to those of modern seawater.

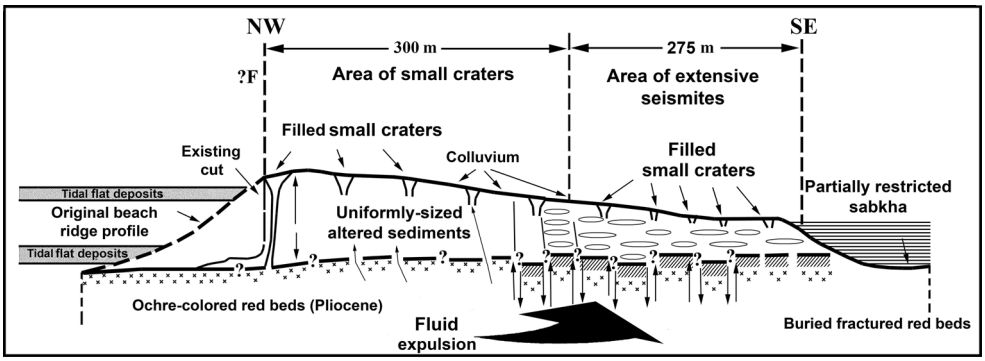

Fig. 7 Schematic cross-section and interpretative model for the features discussed in this study. Fluid expulsion is considered to be coeval with seismic events

Carbonate isotopes

The mud-volcano dolomite does not resemble dolomite from the Persian Gulf sabkhas or from the Dammam Formation aquifer in carbon isotopes (Fig. 6). However, its isotopic composition overlaps with late diagenetic calcite from the Dammam aquifer.

The isotope compositions of water and dissolved bicarbonate in equilibrium with the mud-volcano dolomite and calcite were calculated using fractionation factors from Horita (2014) for oxygen, and data summarized by Ohmoto and Rye (1979) for carbon. The findings are shown in Fig. 6. The temperature range used for the calculations was 50 to 80 °C, consistent with fluid inclusion data for gypsum from other warm-water mud volcanoes. For temperatures of 70–90 °C, the mud-volcano water would have the same range of $\delta^{18}O$ as water in equilibrium with the calcite cement of the Dammam Formation aquifer (calculated from the data by Hanafy et al. 2005), or with sabkha pore water from Kuwait (Robinson and Gunatilaka 1991). Gulf seawater can be in equilibrium with dolomite only at temperatures of 100 °C or greater.

The $\delta^{13}C$ values of dissolved bicarbonate in equilibrium with dolomite (–4 to –8‰; Fig. 6) for the temperature range used here indicate the addition of low-$\delta^{13}C$ bicarbonate to the near-0‰ bicarbonate of marine origin that is clearly present in most of the fields shown in Fig. 6. Low-$\delta^{13}C$ bicarbonate can be generated by oxidation of buried organic matter, in this case most likely as a result of BSR or bacterial reduction of Fe^{3+} (BFR). The bleaching of Fe oxides around the edifice and the presence of spheroidal dolomites at the crest of the mud volcanoes point to localized BFR. The calcite veins are paragenetically younger than the dolomite but, if the calcite and the dolomite formed at similar temperatures, then it is likely that the calcite was in equilibrium with water having $\delta^{18}O$ values 3–4‰ higher than that in equilibrium with the dolomite. Alternatively, they may have formed in equilibrium with Dammam Formation water at a temperature below 50 °C.

Conclusions

These exceptional outcrops comprising sulphate mud volcanoes and seismites preserved in a sabkha are a consequence of several unique conditions (Fig. 7): (1) the area is characterized by earthquakes of low to moderate magnitude; (2) the area is on the eastern flank of the most oil-endowed anticline on Earth; (3) empirical relationships enable linkages between large seismic events and liquefaction events (Ambraseys 1988). The dimensions of liquefaction structures result from a combination of earthquake parameters and sedimentary features. Different methods have been proposed to estimate the severity of earthquakes using liquefaction structures (dykes, fluid expulsion features, mud volcanoes; cf. Allen 1986; Leeder 1987; Castilla and Audemard 2007).

The primary nature of the dolomite spheroids in the matrix suggests an association between the migration of methane and the presence of microbial components in the mud fluids (Gunatilaka 1989). In this context, the present study identifies a hitherto unrecognized formation of mud injections in a shallow tidal-flat environment in the Persian Gulf. These cannot be demonstrated to be related to regional hydrothermal systems (Grasby et al. 2009), unless supporting evidence of high-temperature fluids can be obtained. Nevertheless, the presence of spheroidal dolomite, vein calcites and unusual stable isotope signatures in sulphate points to a sub-mud mound mixing of seawater-derived fluids with sulphate-bearing continental fluids of a deep nature. Stable isotope data in dolomite indicate a role for bacterial reduction of sulphate or Fe^{3+}, and are consistent with a deep origin for water, possibly the Dammam aquifer. The ancient analogues of mud volcanoes in the geological record together with the Kuwait swarm (Gaillard et al. 1992; Campbell et al. 2002) are important scientific targets for evaluating the three-dimensional biological and physical nature of seeps in general.

Acknowledgements This is a self-funded project. The authors would like to thank Kuwait University for providing assistance with transport and access to laboratories for sample preparation and analysis. The manuscript has benefited from useful comments by reviewers. Stable isotope analyses were provided by the Environmental Isotope Laboratory at the University of Arizona.

Conflict of interest The authors declare that they have no conflict of interest.

References

Allen JRL (1986) Earthquake magnitude-frequency, epicentral distance, and soft-sediment deformation in sedimentary basins. Sediment Geol 46:67–75

Al-Shuaibi A, Duane MJ, Mahmoud H (2012) Microbial-activated sediment traps associated with oncolite formation along a peritidal beach, northern Arabian (Persian) Gulf, Kuwait. Geomicrobiology J 29:679–696

Ambraseys NN (1988) Engineering seismology. Earthquake Eng Struct Dynamics 17:1–105

Authemayou CD, Chardon D, Bellier O, Malekzadeh Z, Shabanian E, Abbassi MR (2006) Late Cenozoic partitioning of oblique plate convergence in the Zagros fold-and-thrust belt (Iran). Tectonics, Am Geophys Union 25, TC3002

Bonini M (2009) Elliptical mud volcano caldera as stress indicator in an active compressional setting (Nirano, Pede-Appenine margin, northern Italy). Geology 36:131–134

Brown KM (1990) The nature and hydrogeologic significance of mud diapirs and diatremes for accretionary systems. J Geophys Res 95: 8969–8982

Campbell KA, Farmer JD, Des Marais D (2002) Ancient hydrocarbon seeps from the Mesozoic convergent margin of California: carbonate geochemistry, fluids and palaeoenvironments. Geofluids 2:63–94

Castilla RA, Audemard FA (2007) Sand blows as a potential tool for magnitude estimation of pre-instrumental earthquakes. J Seismol 11:473–487

Chafetz HS, Rush PF (1995) Two-phase diagenesis of Quaternary carbonate, Arabian Gulf: insights from $\delta^{13}C$ and $\delta^{18}O$ data. J Sediment Res A65:294–305

Chafetz HS, Imerito-Tetzlaff A, Zhang J (1999) Stable isotope and elemental trends in Pleistocene sabkha dolomites: descending water vs. sulfate reduction. J Sediment Res 69:256–266

Chiba H, Sakai H (1985) Oxygen isotope exchange rate between sulfate and water at hydrothermal temperatures. Geochim Cosmochim Acta 49:993–1000

Claypool GE, Holser WT, Kaplan IR, Sakai H, Zak I (1980) The age curves of sulfur and oxygen in marine sulfate and their mutual interpretation. Chem Geol 28:199–260

Davies R, Stewart SA (2005) Emplacement of giant mud volcanoes in the South Caspian Basin: 3D seismic reflection imaging of their root zones. J Geol Soc Lond 162:1–4

Deville E, Battani A, Griboulard R, Guerlais SH, Herbin JP, Houzay JP, Muller C, Prinzhofer A (2003) Mud volcanism origin and processes. New insights from Trinidad and the Barbados Prism. In: Van Rensbergen P, Hillis RR, Maltman AJ, Morley C (eds) Subsurface sediment remobilization. Geol Soc Lond Spec Publ 216:475–490

Dupré S, Mascle J, Foucher J-P, Harmegnies F, Woodside J, Pierre C (2014) Warm brine lakes in craters of active mud volcanoes, Menes caldera off NW Egypt: evidence for deep-rooted thermogenic processes. Geo-Mar Lett 34:153–168

Feseker T, Brown KR, Blanchet C, Scholz F, Nuzzo M, Reitz A, Schmidt M, Hensen C (2010) Active mud volcanoes on the upper slope of the western Nile deep-sea fan—first results from the P362/2 cruise of R/V *Poseidon*. Geo-Mar Lett 30:169–186

Gaillard C, Rio M, Rolin Y, Roux M (1992) Fossil chemosynthetic communities related to vents or seeps in sedimentary basins: the pseudobioherms of Southwestern France compared to other world samples. Soc Econ Paleontol Mineral 7:451–465

Gerdes G, Krumbein WE (1987) Biolaminated deposits. Lecture Notes in Earth Sciences 9. Springer-Verlag, Berlin

Grasby SE, Bezys R, Beauchamp B (2009) Silica chimneys formed by low-temperature brine spring discharge. Astrobiology 9:931–941

Graue K (2000) Mud volcanoes in deep water Nigeria. Mar Petrol Geol 17:959–974

Gunatilaka A (1989) Spheroidal dolomites – origin by hydrocarbon seepage? Sedimentology 36:701–710

Hanafy H, Holail MN, Mohammad A, Shabaan AS, Mansour AS, Rifai I (2005) Diagenesis of the middle Eocene upper Dammam subformation, Qatar: petrographic and isotopic evidence. Carbonates Evaporites 20:72–81

Horita J (2014) Oxygen and carbon isotope fractionation in the system dolomite-water-CO_2 to elevated temperatures. Geochim Cosmochim Acta 129:111–124

Hubbert MK, Willis DGW (1957) Mechanics of hydraulic fracturing. Trans Am Inst Min Eng 210:153–168

Jolly R, Lonergan L (2002) Mechanisms and controls on the formation of sand intrusions. J Geol Soc Lond 159:605–617

Judd A, Hovland M (2007) Seabed fluid flow – The impact on geology, biology, and the marine environment. Cambridge University Press, Cambridge

Kendall CG, Skipwith PA (1968) Recent algal mats of a Persian Gulf lagoon. J Sediment Petrol 38:1040–1058

Kopf A (2002) Significance of mud volcanism. Rev Geophys 40(2): 1005–1052

Leeder MR (1987) Sediment deformation structures and the palaeotectonic analysis of sedimentary basins, with a case-study from the Carboniferous of northern England. Geol Soc Lond Spec Publ 29:11–24

Loncke L, Mascle J, Fanil J (2004) Mud volcanoes, gas chimneys, pockmarks and mounds in the Nile deep-sea fan (Eastern Mediterranean): geophysical evidences. Mar Petrol Geol 21:669–689

Lu FH, Meyers WJ, Schoonen MA (2001) S and O (SO_4) isotopes, simultaneous modeling, and environmental significance of the Nijar Messinian gypsum, Spain. Geochim Cosmochim Acta 65: 3081–3092

McKenzie JA (1981) Holocene dolomitization of calcium carbonate sediments from the coastal sabkhas of Abu Dhabi, UAE: a stable isotope study. J Geol 89:185–198

Morley CK (2002) Structural Geology of the Berakas Syncline - Regional Reservoir Scale Perspectives. University Brunei Darussalam, Department of Petroleum Geosciences, Report (Field trip guide) Brunei Shell, Brunei

Morley CK (2003) Outcrop examples of mudstone intrusions from the Jerudong Anticline. In: Van Rensbergen P, Hillis RR, Maltman AJ, Morley CK (eds) Subsurface sediment remobilization. Geol Soc Lond Spec Publ 216:381–394

Morley CK, Crevello P (1998) Shale tectonics associated with active diapirism; the Jerudong Anticline, Brunei Darussalam. J Geol Soc Lond 155:1154–1170

Mount JF (1993) Formation of fluidization pipes during liquefaction: examples from Uratanna Formation (Lower Cambrian), South Australia. Sedimentology 40:1027–1037

Mukhopadhyay A, Al-Sulaimi J, Al-Awadhi E, Al-Ruwaih F (1996) An overview of the Tertiary geology and hydrogeology of the northern part of the Arabian Gulf region with special reference to Kuwait. Earth Sci Rev 40:259–295

Murton BJ, Biggs J (2003) Numerical modelling of mud volcanoes and their flows using constraints from the Gulf of Cadiz. Mar Geol 195: 223–236

Negaresh H, Khosravi M (2008) The geomorphic and morphometrics of the Napag Mud Volcano in the south eastern area of Iran. University Isfahan, J Humanities 30:51–68

Ohmoto H, Rye RO (1979) Isotopes of sulfur and carbon. In: Barnes HL (ed) Geochemistry of hydrothermal ore deposits. Wiley, New York, pp 509–567

Olsen ER (1975) Oxygen and sulfur isotope geochemistry of marine evaporates. Open Access Dissertations and Theses, Paper 849

Roberts KS, Davies RJ, Stewart SA (2010) Structure and exhumed mud volcano feeder complexes, Azerbaijan. Basin Res 22:439–451

Robertson AHF, Kopf A (1998) Tectonic setting and processes of mud volcanism on the Mediterranean Ridge accretionary complex: evidence from Leg 160. In: Robertson AHT, Emeis KC, Richter C et al (eds) Proc Ocean Drilling Program, Scientific Results 160. Ocean Drilling Program, College Station, TX, pp 665–680

Robinson BW, Al-Ruwaih F (1985) The stable isotope composition of water and sulfate from the Raudhatain and Umm al Aish freshwater fields, Kuwait. Chem Geol 58:29–136

Robinson BW, Gunatilaka A (1991) Stable isotope studies and the hydrological regime of sabkhas in southern Kuwait, Arabian Gulf. Sediment Geol 73:141–159

Sadek AW (2004) Seismic map for the State of Kuwait. Emirates J Eng Res 9:53–58

Seilacher A (1969) Fault-graded beds interpreted as seismites. Sedimentology 13:155–159

Stewart SA, Davies RJ (2006) Structure and emplacement of mud volcano systems in the South Caspian Basin. AAPG Bull 90:771–786

Uchupi E, Swift SA, Ross DA (1996) Gas venting and late Quaternary sedimentation in the Persian (Arabian) Gulf. Mar Geol 129:237–269

Van Rensbergen P, Morley CK, Ang DW, Hoan TQ, Lam NT (1999) Structural evolution of shale diapirs from reactive rise to mud volcanism: 3D seismic data from the Baram delta, offshore Brunie Darussalam. J Geol Soc Lond 156:633–650

Wood WW, Sanford WE, Al Habshi ARS (2002) Source of solutes to the coastal sabkha of Abu Dhabi. Geol Soc Am Bull 114:259–268

Yamamoto JK, Fairchild TR, Boggiani PC, Montanheiro TJ, de Araujo CC, Kiyohara PK, de Matos SLF, Soares PC (2005) A record of Permian subaqueous vent activity in southeastern Brazil. Nature 438:205–207

Yechieli Y, Wood WW (2002) Hydrogeologic processes in saline systems: playas, sabkhas, and saline lakes. Earth Sci Rev 58:343–365